Multiphysics analysis for fluid-structure interaction of flexible baffle inside wavy cavity with slipping wall

Mohammed Wahhab Al-Jibory
University of Kerbala
Mokdad Hayawi Rahman (mokdad.jwad.uob@gmail.com)
Al-Farahidi University

Research Article

Keywords: Fluid–structure interaction analysis, COMSOL Multiphysics, lid-driven cavity, Flexible wall

Posted Date: June 23rd, 2022

DOI: https://doi.org/10.21203/rs.3.rs-1771449/v1

Abstract

The development of methods for making fluids in a state of turbulence to obtain better heat transfer and its strong effect on the elastic wall. One of the ways that we can obtain the turbulent state of the fluid is to make one of the surfaces of the solid slide at a certain speed. This slip leads to the surface tension in a state of turbulence, and this rotates the fluid flow in a way large and in order to obtain better turbulence, it is used to make the surfaces surrounding the fluid in a directional way to help rotate the fluid. The results proved the effectiveness of this stereotype, as the force of the effect of the fluid velocity on the elastic wall was in the case of the thickness of 0.5 mm and the sliding velocity of 0.9 m/s, where the deformation was 5.6 mm, which is the best strike condition was deduced either at 2 mm thickness and 0.1 m/s sliding velocity where the deformation was 0.272 mm which is the least deformation reached by the wall.

1. Introduction

An examination of consistent laminar blended convection heat move in a cover driven cavity with an adaptable base surface is investigated. The aftereffects of this examination uncovered that the versatility of the base divider surface assumes a huge part on the hotness move improvement. This clears the street for future exploration studies to think about adaptable dividers when augmentation of heat move is looked for [1]. Mathematical examination of consistent laminar blended convection stream and hotness move in a top driven cavity with an adaptable warmed base surface is researched. For an adaptable base divider case, a completely coupled liquid construction cooperation (FSI) examination is used and the liquid area is portrayed by an Arbitrary-Lagrange-Eulerian (ALE) detailing. This examination shows the advantages of using adaptable dividers when expansion of hotness move is looked for at high Grashof numbers [2]. The presence of deformable (versatile) dividers further develops the hotness move rate by 17% contrasted and unbending (opening) dividers in a pit chamber, concentrate on finds. The job of the versatile divider is articulated at Ri = 10 and the administering conditions of association among liquid and flexible divider are tackled utilizing an Arbitrary Lagrange-Eulerian approach with Finite Element technique [3]. A flexible balance is appended to a hot vertical mass of a square depression and is exposed to lightness powers. Expanding the nondimensional abundancy the wavering blade can altogether upgrade the Nusselt number. A balance length of 0.2 can be considered as the best length for heat move upgrade and compatible with different swaying amplitudes [4]. The blended convection peculiarity inside the fenced in areas remembered by moving divider has numerous applications for ventures. This article presents an itemized audit on the blending of different pits in with various shapes, limit conditions and chiefly nanofluid-filled which have functional applications. The impacts of actual limit conditions, for example, moving dividers, tendency points and outer attractive power are examined. Different popular calculation strategies and related calculations are acquired [5]. The current paper examines the job of liquid construction association (FSI) in the blended convection inside a square pit having two channel and outlet openings. Conditions administer the unsteady fields of liquid, warm and focuses are addressed mathematically utilizing the Galerkin Finite Element Method executed in Arbitrary

Lagrange - Eularian approach. The results show that the adaptable balance improves the Nusselt number better compared to the inflexible balance. Be that as it may, at extremely high upsides of Richardson number, the balance material ought not beavery flexible [6]. Mathematical examination is performed over the top driven hexagon depression loaded up with water that is somewhat warmed at the upper divider, that is moving with uniform speed. The result reveals that the hotness length, Richardson number and Reynold number are unequivocally connected with heat move. The round obstruction assumed a significant part in the arrangement of isotherms by changing the different requirement at the surface [7]. Increase of energy transport in various designing gadgets can be settled by utilization of different blades inside the gadget and compelling hotness move specialist. Convective energy transport inside a square walled in area having a mounted adiabatic blade and interior strong square affected by moving upper line and alumina/water nano liquid has been examined. It has been uncovered that the inner square area and nanoparticles focus can handle the power of hotness transfer [8]. Force-criticism gadgets, alongside computer generated reality, are being read up for applications connected with amusement and restoration. These gadgets by and large include either direct drive engines or engines with decrease gear. In spite of the fact that unbending nature can be increased with decrease gears, they diminish back-drivability and limit the movement opportunity of the gadget. To address these problems, we fostered a coercively feeding gadget activated with a magnetorheological grip and pneumatic fake muscles that can flawlessly fluctuate its solidness and consistency [9]. An inundated limit limited contrast cross section Boltzmann is proposed to recreate liquid design association of viscoelastic liquids. The Bingham model with next to no regularization of the constitutive regulation was applied. The exactness of the technique has been approved in a cover driven pit. In these examinations, the yielded/unyielded segments and smoothest out have been portrayed for high Rayleigh numbers [10]. The point of this paper is to examine the impact of MHD blended convection flow of Cu-water nanofluid in a trapezoidal top driven depression with various slant points in a scope of 0° to 60°. The overseeing conditions of the stream by utilizing the limited volume strategy and SIMPLE calculation have been mathematically tackled. Results show that the normal Nusselt number on the non-consistently warmed base divider is dependent on dimensionless boundaries and slant points. Likewise, applying an attractive field, diminish the speed profile changes, and using nanoparticles will cause expanding the Nusselt number [11]. Sound waving cooperation's among vegetation and liquid streams are known to emerge under conditions related with the blending layer unsteadiness. A comparative movement has likewise been seen in stream control applications, where passive slender structures are utilized to expand feign body wakes. This work researches the coupled interactions of an enormous cluster of slim designs in an open-channel stream, via numerical recreation [12]. Paper researches the blended convection heat move of nonnewtonian liquid construction collaboration inside an open trapezoidal pit. Mathematical reproduction is accomplished utilizing limited component technique with erratic Lagrange-Eulerian plot. Results show that at Re = 300, Nusselt number of a firm balance is 2.6% and 7% higher than that of milder adaptable blade for n = 0.5–1.5 [13]. In this review, normal convection and entropy age investigation of nanofluid inside a slanted depression including a bended formed conductive parcel are. performed under the effect of slanted attractive field by utilizing Galerkin in weighted remaining limited component strategy. Mathematical recreations are performed for different upsides of Rayleigh number (somewhere in the range of 104 and 106), tendency

point of the pit (somewhere in the range of 0^o and 180^o) and Hartmann number somewhere in the range of 0 and 50 [14]. A thought of penetrable (attractions/infusion) chamber is proposed to control the optional vortices showing up in the notable top driven pit stream through the water-based ferrofluids. The force of attractive source can modify the framework in such a manner to adjust the stream and to move the liquid away from the magnetic source area. It likewise decreases the stacking consequences for the dividers of the cavity [15]. Organs-on-Chip innovation plans to address this need by utilizing propels in microfabrication and biomaterials. The Open-Top Chip configuration has the ability to fuse a tissue-explicit extracellular grid gel and imitate the compositional intricacy of tissues. We likewise give confirmation of-idea information on the plausibility of utilizing the framework with essential human skin and alveolar epithelial cells [16]. The impact of an attractive field on hotness and liquid progression of ferrofluid in a helical cylinder is concentrated mathematically. Parametric examinations are done to research the impacts of various factors, for example, the attractive field slope worth and Reynolds number on heat move rate and tension drop. There is an ideal case for warm water powered execution which brings about most top performance of helical cylinders within the sight of a solid attractive field [17]. Convection in a cubical permeable compartment has been constrained by permitting the base divider to be of wavy shape and by embedding a conductive square chamber within it. This control cycle has been examined briefly in an alumina-water nanofluid. Isothermal circumstances are forced at the base wavy divider (cold) as well as at the upward dividers (hot) [18]. In the current review, the free convection heat move of a power-regulation non-Newtonian fluid is considered in a hole containing a flexible hot slender radiator. The conditions administering fluid forward heat move are addressed utilizing the finite component technique with a programmed time-venturing plan. Moving the radiator up disintegrates the hotness transfer rate by smothering the convection few forces. Increasing the length of the component is additionally found to lessen the normal Nusselt number and to expand the strains in the radiator [19].

2. Originality

The previous research works on a separate study of the case, meaning that in some researches a study is conducted on the wavy wall and some research works on the sliding wall and some research on the flexible wall, the originality in this research paper works to collect all the ideas through previous studies and collect them in one model and study it and narrate the changes that occur in the fluid and its turbulence.

3. Methodology

Where the model was designed with the SoildWorks program, which is a program dedicated to precise engineering design, with dimensions of length 100 mm, width 100 mm, and height 100 mm, and the work is three-dimensional, where the surrounding surfaces are a wave with wavelength 50 mm.

After the process of designing the model, it is necessary to make a grid for the model to obtain accurate results that can be adopted, as work was done on the reliability of the mesh and the increase in the number of the element until reaching stable results that do not change with the increase in the number of

the element, where stability was obtained in the conclusions at the number of elements was 854675 in max deformation 0.0056 m.

Table (1): Mesh independency.

Case	Element	Deformation max. (M)
1	201467	0.0034
2	423406	0.0051
3	634234	0.0055
4	854675	0.0056

Where the COMSOL Multiphysics program was used to make this simulation, which is one of the exact engineering simulation programs, where the FSI processor was used, which is linking the fluid movement side with the stress measurement processor on the flexible wall, where the fluid was used as water and made the upper surface sliding at a variable speed that was (0.1, 0.3, 0.5, 0.7, 0.9) m/s As for the flexible wall, a different thickness was used for each case, where (0.5, 1, 2) mm was used, where the simulation process was carried out at a time of 1.5 s with a time step of 0.005 s to see the clear changes of the simulation process and the fluid flow and the effect on the wall.

4. Governing Equations

The equation for the condition of motion is as follows:

$$\frac{\partial \rho}{\partial t} + \nabla \cdot \left(\rho \vec{v}\right) = S_m$$

1

…….

In equation one it is in the case of general motion, but in Eq. 2 the equation is in the form of a direction, that is, it is in a special case, as it is given in the following form

$$\frac{\partial \rho}{\partial t} + \frac{\partial}{\partial x}\left(\rho v_x\right) + \frac{\partial}{\partial r}\left(\rho v_r\right) + \frac{\rho v_r}{r} = S_m$$

2

…….

where x is the essential heading, r is the winding bearing, v_x is the center speed, and v_r is the extended speed.

Insurance of power in an inertial (non-accelerating)

$$\frac{\partial }{\partial t}\left(\rho \overrightarrow{v}\right)+\nabla \cdot \left(\rho \overrightarrow{v}\overrightarrow{v}\right)=-\nabla p+\nabla \cdot \left(\stackrel{-}{\stackrel{\rightarrow}{\tau }}\right)+ \rho \overrightarrow{g}+\overrightarrow{F}$$

3

…….

where p is the static strain, $\stackrel{-}{\stackrel{\rightarrow}{\tau }}$ is the tension tensor (portrayed underneath), and $\overrightarrow{{\rho }\text{g}}$ and$\overrightarrow{F}$ are the gravitational body power and outside body powers (for example, that rise out of association with the dissipated stage), independently. $\overrightarrow{F}$ in like manner contains other model-subordinate source terms, for instance, porous media and customer described sources. The strain tensor $\stackrel{-}{\stackrel{\rightarrow}{\tau }}$is given by:

$$\stackrel{-}{\stackrel{\rightarrow}{\tau }}=\mu \left[\left(\nabla \overrightarrow{v}+\nabla {\overrightarrow{v}}^{T}\right)-\frac{2}{3}\nabla \cdot \overrightarrow{v}I\right]$$

4

……..

where μ is the nuclear consistency, I is the unit tensor, and the second term on the right hand side is the effect of volume extension.

For 2D axisymmetric computations, the center point and extended power assurance conditions are given by:

$$\begin{array}{rr}\frac{\partial }{\partial t}\left(\rho {v}_{x}\right)+\frac{1}{r}\frac{\partial }{\partial x}\left(r\rho {v}_{x}{v}_{x}\right)+\frac{1}{r}\frac{\partial }{\partial r}\left(r\rho {v}_{r}{v}_{x}\right)=& -\frac{\partial p}{\partial x}\\ & +\frac{1}{r}\frac{\partial }{\partial x}\left[r\mu \left(2\frac{\partial {v}_{x}}{\partial x}-\frac{2}{3}(\nabla \cdot \overrightarrow{v})\right)\right]\\ & +\frac{1}{r}\frac{\partial }{\partial r}\left[r\mu \left(\frac{\partial {v}_{x}}{\partial r}+\frac{\partial {v}_{r}}{\partial x}\right)\right]+ {F}_{x}\end{array}$$

5

…

And

$$\begin{array}{rr}\frac{\partial }{\partial t}\left(\rho {v}_{r}\right)+\frac{1}{r}\frac{\partial }{\partial x}\left(r\rho {v}_{x}{v}_{r}\right)+\frac{1}{r}\frac{\partial }{\partial r}\left(r\rho {v}_{r}{v}_{r}\right)=& -\frac{\partial p}{\partial r}\\ & +\frac{1}{r}\frac{\partial }{\partial x}\left[r\mu \left(\frac{\partial {v}_{r}}{\partial x}+\frac{\partial {v}_{x}}{\partial r}\right)\right]\\ & +\frac{1}{r}\frac{\partial }{\partial r}\left[r\mu$$

\left(2\frac{\partial {v}_{r}}{\partial r}-\frac{2}{3}(\nabla \cdot \overrightarrow{v})\right)\right]\\ & -2{\mu }_{{r}^{r}}^{{v}_{r}}+\frac{2}{3}\frac{\mu }{r}(\nabla \cdot \overrightarrow{v})+\rho \frac{{v}_{r}}{r}+{F}_{r}\end{array}

6

..

where

\nabla \cdot \overrightarrow{v}=\frac{\partial {v}_{x}}{\partial x}+\frac{\partial {v}_{r}}{\partial r}+\frac{{v}_{r}}{r}

7

…….

what's more {v}_{z} is the whirl speed.

5. Results And Discussion

The results will be reviewed in two parts, the first with the change in wall thickness and knowledge of its effect, and the second with the difference in the speed of wall sliding and the effect on the stresses and the speed of flow.

5.1 Effect of wall thickness on stress and deformation

Where we note from the following figures the effect of wall sliding velocity on the thickness of the elastic wall, as the elastic wall at 0.5 mm thickness had the most deflection and gave sufficient wiper for fluid vortices to pass, but in the rest of the cases, the deformation of the elastic wall is little as it does not give ample space for the fluid to flow.

Through the forms of deformation of the flexible wall, the increase in the thickness of the wall gives less deformation than the speed of wall sliding. We note that the deformation at 0.5 mm thickness has the largest amount of deformation, where the deformation reached 0.0056 m, while at thickness 2 mm, the deformation reached 0.00103 m, which is the least deformation for the rest of the cases.

It is natural that the increase in deformation is due to the effect of sliding the upper wall and due to the thickness of the wall, the resulting stress follows the deformation in the same way, as the maximum value of the stress was reached at the case where the wall thickness was 0.5 mm, where the stress reached 500 N/m^2. Where the thickness is 2 mm, the stress is 30 N/m^2, which is the lowest value of the stresses reached in this case compared to the rest of the cases.

5.2 The effect of the speed of sliding the upper wall on the stresses and velocity

From the following figure, we note the effect of the upper wall sliding velocity on the vortex velocity that causes deformation of the elastic wall. We note that the upper wall sliding velocity when its velocity is 0.1 m/s, the vortex velocity at that velocity is 0.05 m/s, which is relatively little. The upper wall is 0.9 m/s, so the vortex velocity of the fluid reached 0.42 m/s, which is considered the largest velocity reached by the vortex, and its weight is more deformed.

The increase in the velocity of sliding of the upper wall increases the velocity of the vortex as we hugged it through the previous figures. Therefore, the deformation of the elastic wall becomes larger as the value of the deformation increases with the increase in the velocity of the upper wall sliding, as the deformation is greater than the velocity of the sliding of the upper wall was 0.1 m/s. It has 0.000172 m, which is the least deformation compared to the rest of the cases. At the velocity of sliding the upper wall is 0.9 m/s, the deformation reached 0.005 m, which is the highest value of the deformation reached by this sliding velocity.

It is known that the increase in deformation leads to an increase in the value of the stresses, as the increase in the velocity of sliding the upper wall increases the stresses gradually with the increase in the velocity value of the upper wall sliding. The value of the stresses is 14 N/m^2, which is the value of a few stresses compared to the rest of the cases, but at the velocity of sliding the upper wall is 0.9 m/s, the value of the stresses reached 500 N/m^2, which is the largest value reached by the stresses due to the effect of the velocity of sliding the upper wall.

6. Conclusion

The increase in fluid turbulence needs a certain way to increase heat transfer and its effect on the elastic wall in the deformation. Work was done on a model that contains a flexible wall and a sliding upper wall at different speeds, as well as a flexible wall of different thickness in the cases where the results proved as follows:

1. The increase in the velocity of sliding the upper wall increases the vortex velocity of the fluid, when the velocity of the flow is 0.9 m/s the speed of the vortex reached 0.42 m/s, which is the largest speed the vortex has reached during the cases.
2. The increase in the velocity of sliding of the upper wall leads to an increase in the velocity of vortices, which increases the deformation of the elastic wall, where the deformation reached at the velocity of sliding of the upper wall 0.9 m/s to 0.0056 m, which is the largest deformation reached by the elastic wall.
3. The decrease in the thickness of the elastic wall leads to an increase in the deformation values, as the minimum deformation value was at the thickness of 2 mm, where the deformation at the sliding velocity of the upper wall 0.9 m/s reached 0.000103 m, which is the lowest case the deformation reached.
4. The increase in the deformation value due to the effect of the sliding velocity of the upper wall leads to an increase in the value of the stresses, where the stress reached at the thickness of 0.5 mm and

the velocity of the upper wall sliding 0.9 m/s to 500 N/m^2, which is the highest deformation reached by the elastic wall during the different cases.

Declarations

Compliance with Ethical Standards

Funding: This research has not received any funding source.

Conflict of Interest: The authors have no affiliation with any organization with a direct or indirect financial interest in the subject matter discussed in the manuscript.

Ethical approval: This article does not contain any studies with human participants conducted by any of the authors.

References

1. Abdalla Al-Amiri; Khalil Khanafer (2011) *Fluid–structure interaction analysis of mixed convection heat transfer in a lid-driven cavity with a flexible bottom wall., 54(17–18), 3826–3836.* doi:10.1016/j.ijheatmasstransfer.2011.04.047
2. Khanafer K (2014) Comparison of flow and heat transfer characteristics in a lid-driven cavity between flexible and modified geometry of a heated bottom wall. Int J Heat Mass Transf 78:1032–1041. doi:10.1016/j.ijheatmasstransfer.2014.07.065
3. Sabbar WA, Ismael MA, Almudhaffar M(2018) *Fluid-structure interaction of mixed convection in a cavity-channel assembly of flexible wall. International Journal of Mechanical Sciences, 149, 73–83.* doi:10.1016/j.ijmecsci.2018.09.041
4. Ghalambaz M, Jamesahar E, Ismael MA, Chamkha AJ(2017) *Fluid-structure interaction study of natural convection heat transfer over a flexible oscillating fin in a square cavity. International Journal of Thermal Sciences, 111, 256–273.* doi:10.1016/j.ijthermalsci.2016.09.001
5. Hemmat Esfe M, Saedodin S, Hasani Malekshah E, Babaie A, Rostamian H (2018) Mixed convection inside lid-driven cavities filled with nanofluids. J Therm Anal Calorim. doi:10.1007/s10973-018-7519-x
6. Ismael MA, Jasim HF(2017) *Role of the Fluid-Structure Interaction in Mixed Convection in a Vented Cavity. International Journal of Mechanical Sciences, S0020740317322348–.* doi:10.1016/j.ijmecsci.2017.11.001
7. Haq RU, Soomro FA, Wang X, Tlili I(2020) *Partially heated lid-driven flow in a hexagonal cavity with inner circular obstacle via FEM. International Communications in Heat and Mass Transfer, 117, 104732–.* doi:10.1016/j.icheatmasstransfer.2020.104732
8. Shulepova EV, Sheremet MA, Oztop HF, Abu-Hamdeh N(2020) *Mixed convection of Al2O3–H2O nanoliquid in a square chamber with complicated fin. International Journal of Mechanical Sciences,*

165, 105192–. doi:10.1016/j.ijmecsci.2019.105192

9. Okui M, Kobayashi M, Yamada Y, Nakamura T (2019) Delta-Type 4-DOF Force-Feedback Device Composed of Pneumatic Artificial Muscles and Magnetorheological Clutch and its Application to Lid Opening. Smart Mater Struct –. doi:10.1088/1361-665X/ab192a
10. Kefayati GHR, Tang H, Chan A(2018) *Immersed Boundary-Finite Difference Lattice Boltzmann method through fluid–structure interaction for viscoplastic fluids. Journal of Fluids and Structures, 83, 238–258.* doi:10.1016/j.jfluidstructs.2018.09.007
11. Toghraie D(2019) *Numerical simulation on MHD mixed convection of Cu-water nanofluid in a trapezoidal lid-driven cavity. International Journal of Applied Electromagnetics and Mechanics, 1–28.* doi:10.3233/JAE-190123
12. O'Connor J, Revell A (2019) Dynamic interactions of multiple wall-mounted flexible flaps. J Fluid Mech 870:189–216. doi:10.1017/jfm.2019.266
13. Yaseen DT, Ismael MA(2020) *Analysis of Power Law Fluid-Structure Interaction in an Open Trapezoidal Cavity. International Journal of Mechanical Sciences, 105481–.* doi:10.1016/j.ijmecsci.2020.105481
14. Selimefendigil F, Öztop HF(2019) *Effects of conductive curved partition and magnetic field on natural convection and entropy generation in an inclined cavity filled with nanofluid. Physica A: Statistical Mechanics and its Applications, 123004–.* doi:10.1016/j.physa.2019.123004
15. Siddiqui AA, Turkyilmazoglu M(2019) *A New Theoretical Approach of Wall Transpiration in the Cavity Flow of the Ferrofluids. Micromachines, 10(6), 373–.* doi:10.3390/mi10060373
16. Varone A, Nguyen JK, Leng L, Barrile R, Sliz J, Lucchesi C, Hinojosa CD(2021) *A novel organ-chip system emulates three-dimensional architecture of the human epithelia and the mechanical forces acting on it. Biomaterials, 275, 120957.* doi:10.1016/j.biomaterials.2021.1
17. Mousavi SM, Jamshidi N, Rabienataj-Darzi AA (2019) Numerical investigation of the magnetic field effect on the heat transfer and fluid flow of ferrofluid inside helical tube. J Therm Anal Calorim –. doi:10.1007/s10973-019-08066-2
18. Alsabery AI, Ismael MA, Chamkha AJ, Hashim I, Abulkhair H(2020) *Unsteady flow and entropy analysis of nanofluids inside cubic porous container holding inserted body and wavy bottom wall. International Journal of Mechanical Sciences, 106161–.* doi:10.1016/j.ijmecsci.2020.106161
19. Ghalambaz M, Mehryan SAM, Feeoj RK, Hajjar A, Hashim I, Mahani B, Roohollah (2020) Free convective heat transfer of a non-Newtonian fluid in a cavity containing a thin flexible heater plate: an Eulerianâ-Lagrangian approach. J Therm Anal Calorim –. doi:10.1007/s10973-020-10292-y

Figures

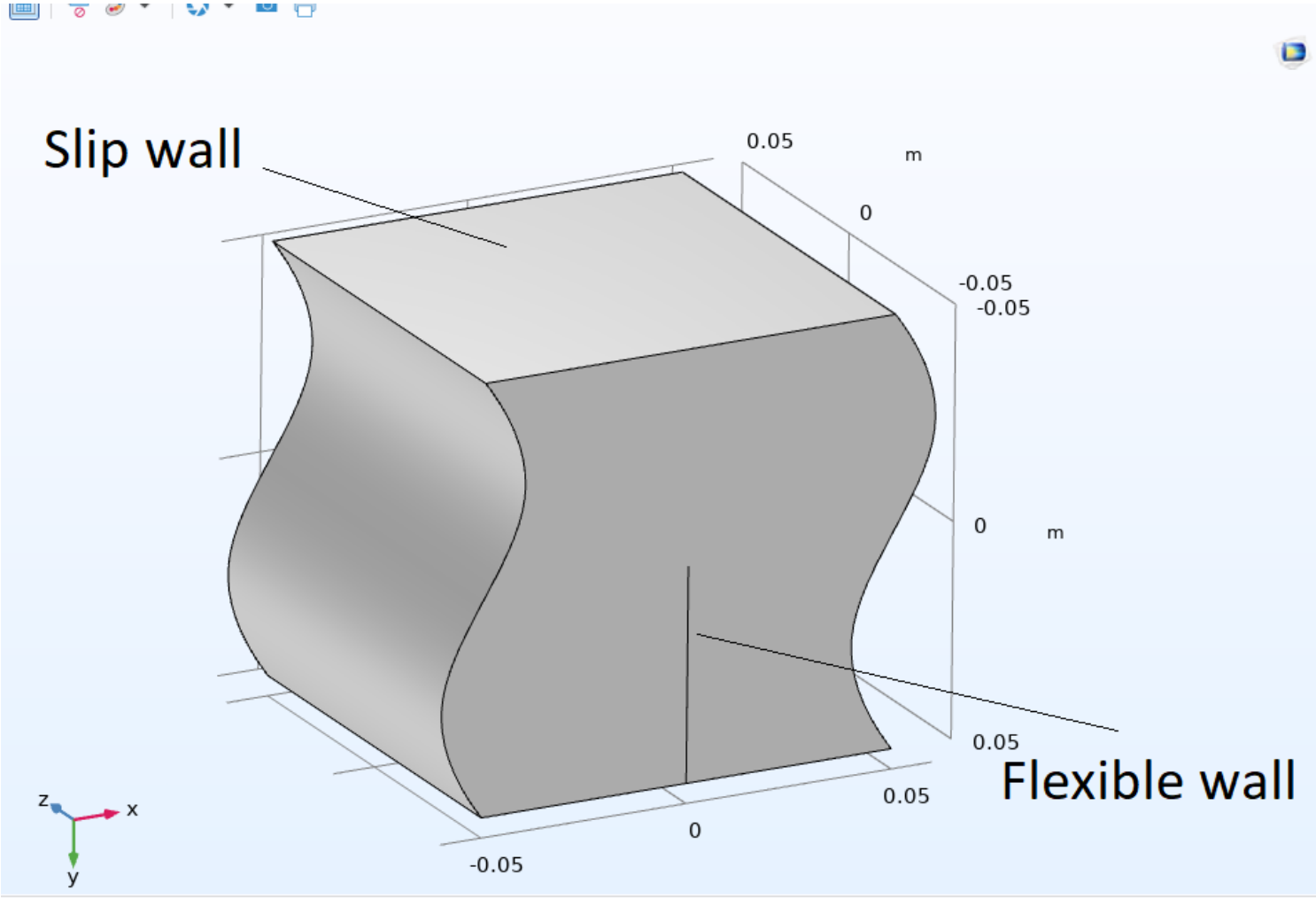

Figure 1

Boundary condition of geometry.

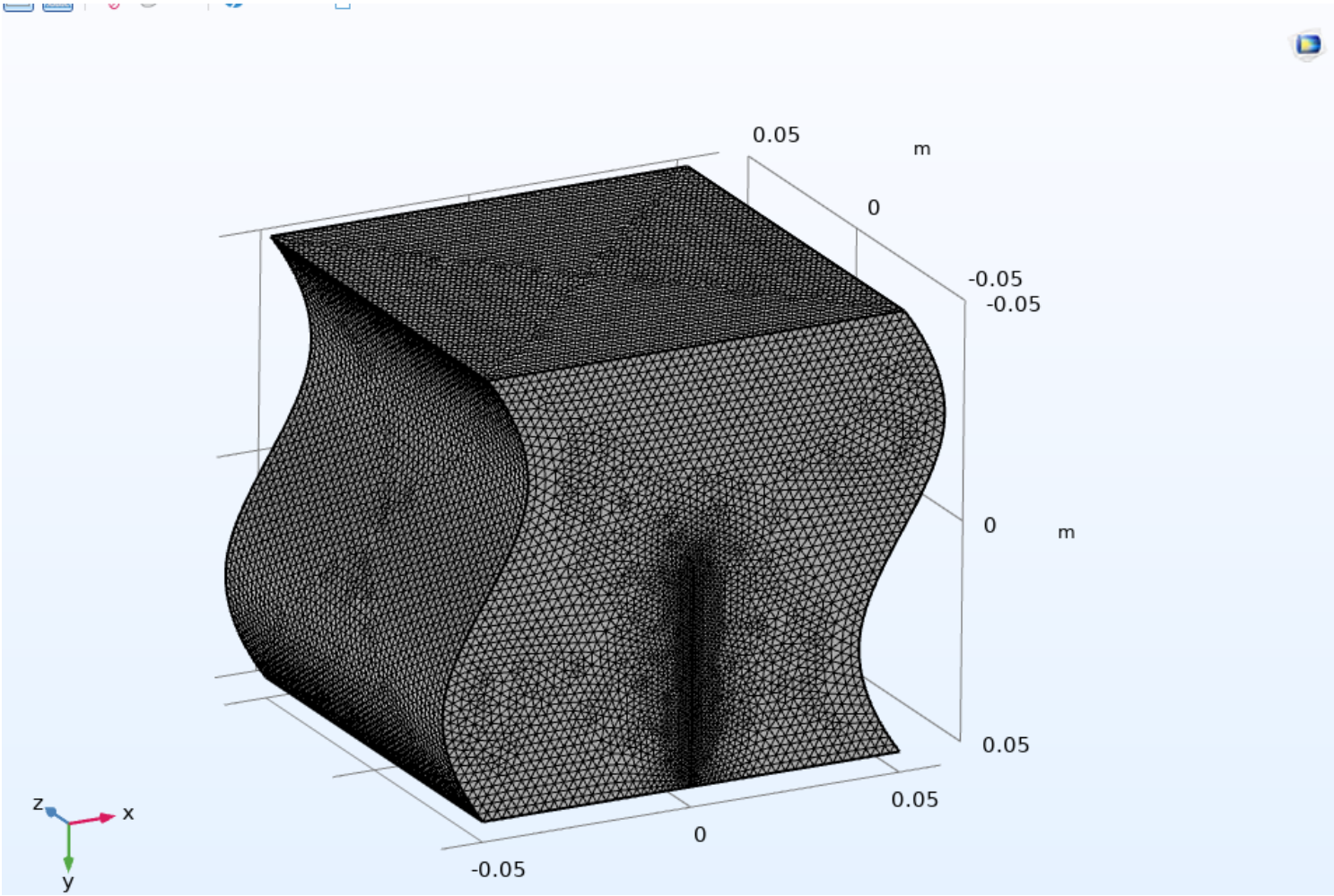

Figure 2

Mesh geometry

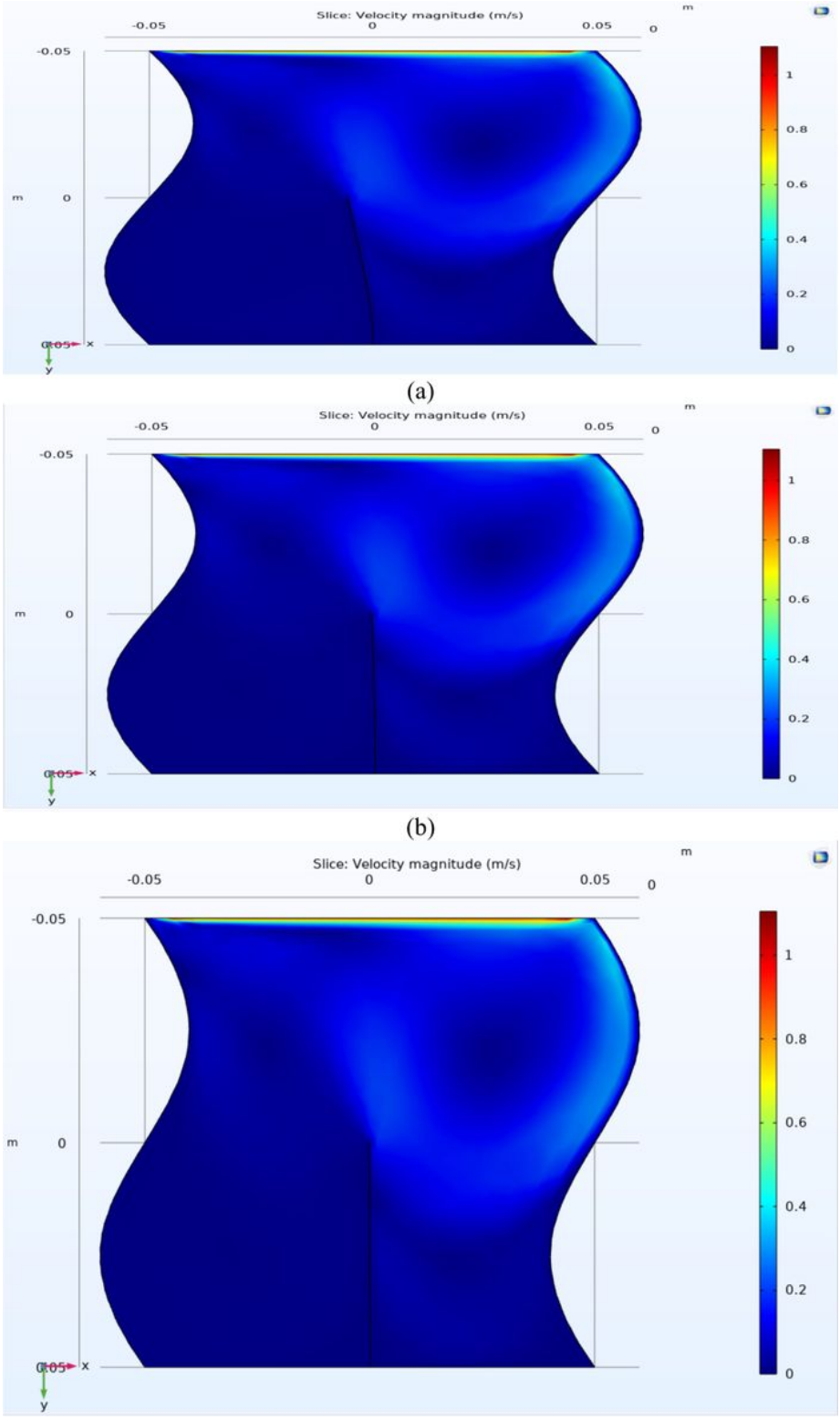

Figure 3

Velocity contour at sliding upper wall 0.9 m/s. (a) 0.5 mm, (b) 1 mm, (c) 2 mm.

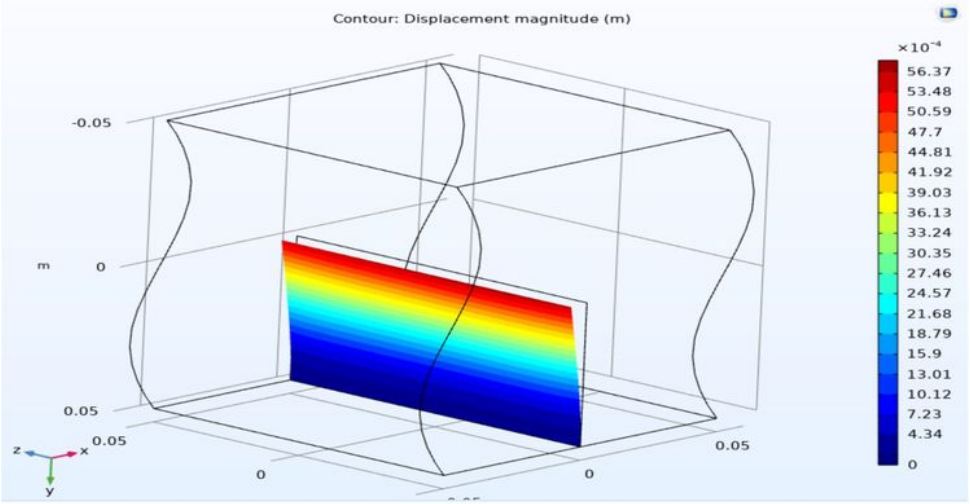

(a)

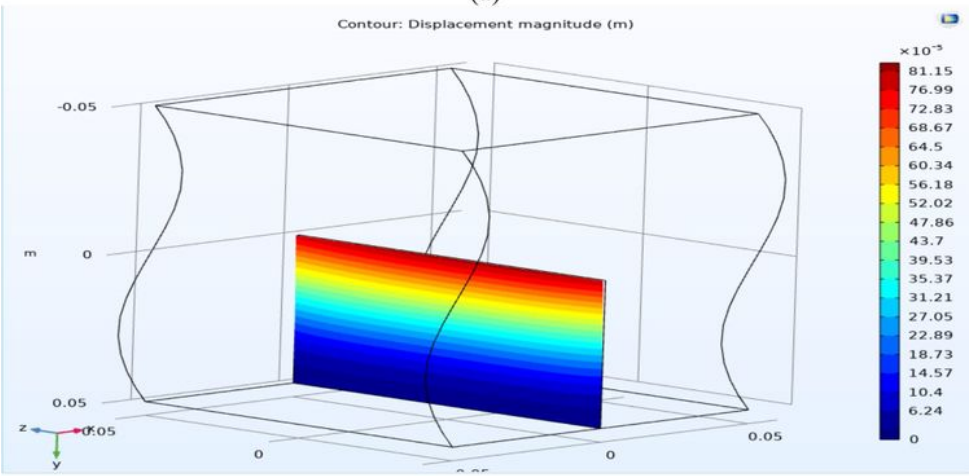

(b)

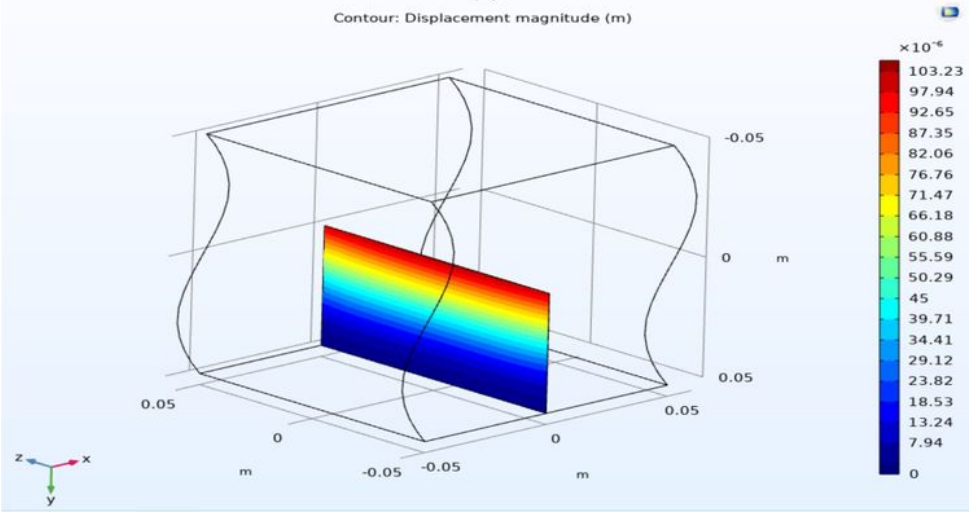

Figure 4

Deformation contour at sliding upper wall 0.9 m/s. (a) 0.5 mm, (b) 1 mm, (c) 2 mm.

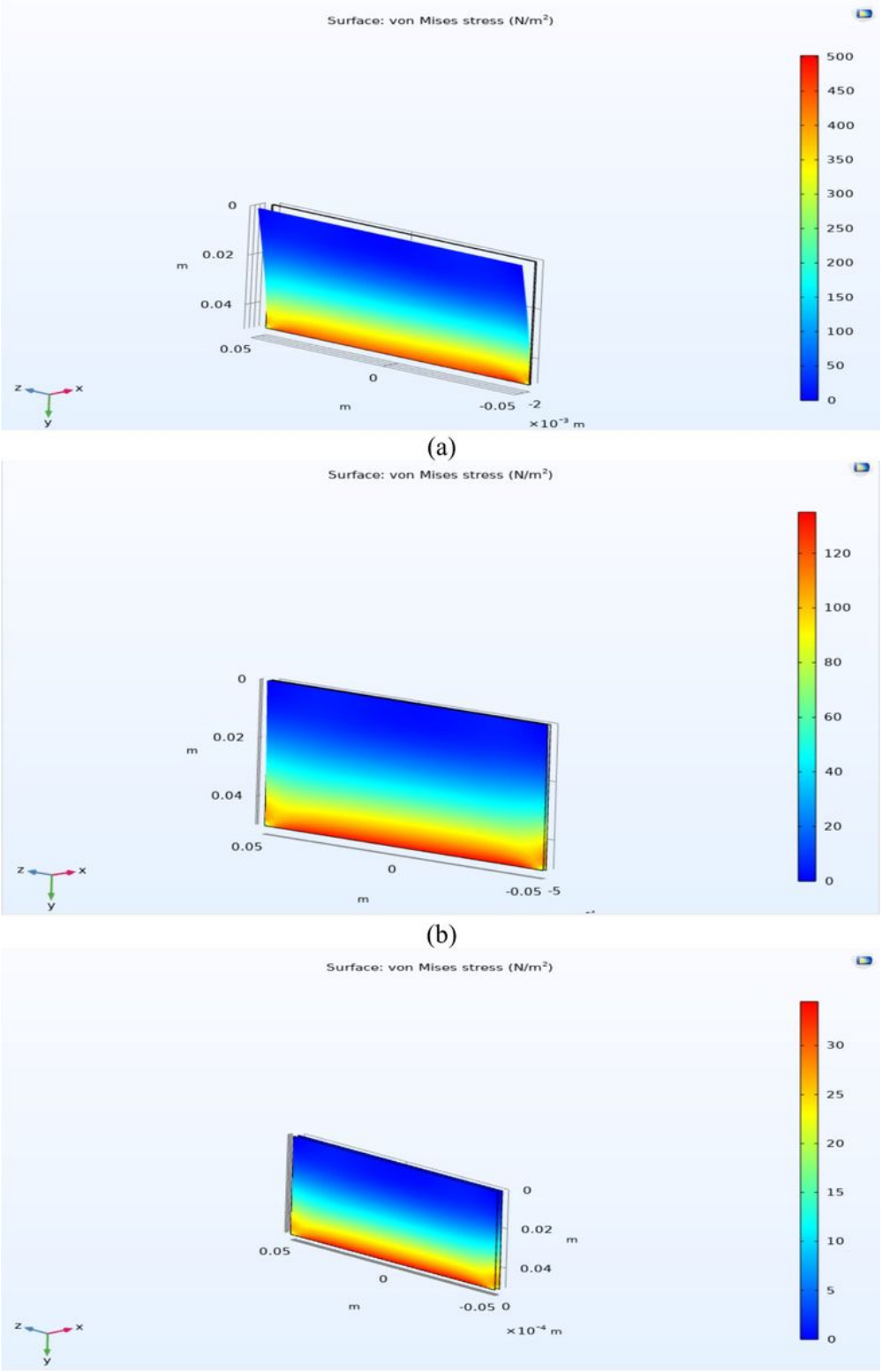

Figure 5

Von mises stress contour at sliding upper wall 0.9 m/s. (a) 0.5 mm, (b) 1 mm, (c) 2 mm.

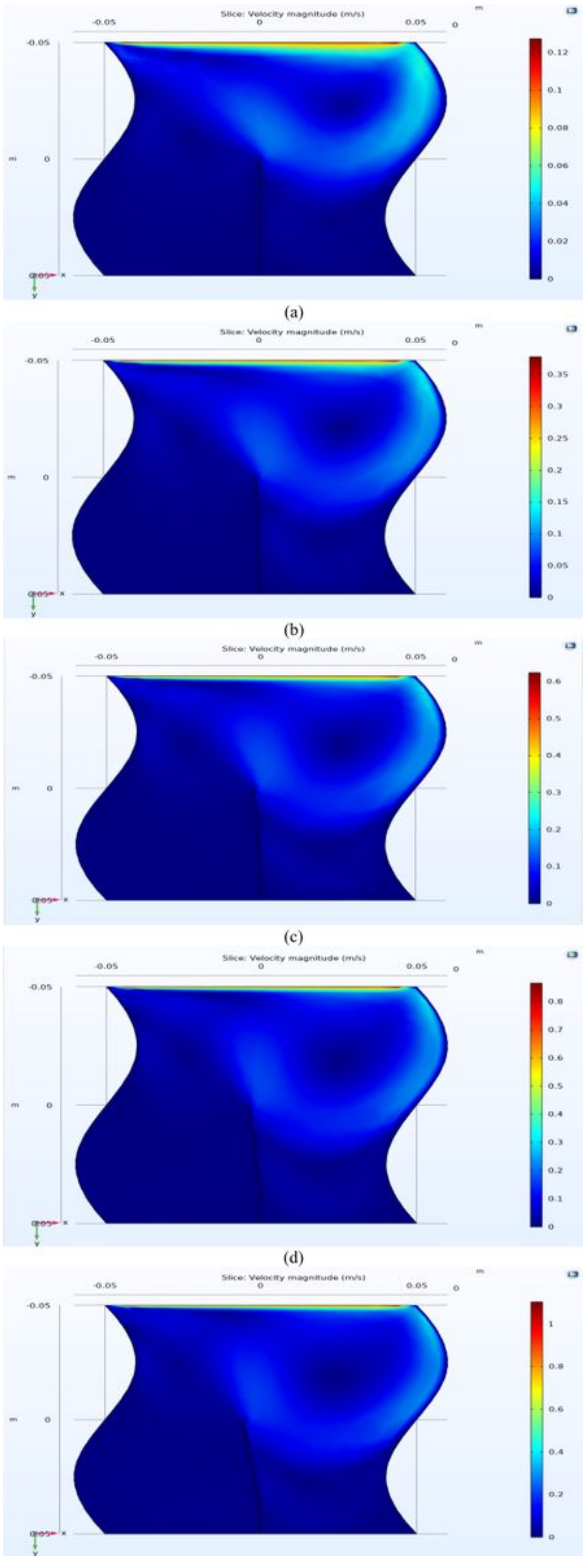

Figure 6

Velocity contour at thickness 0.5 mm. (a) 0.1 m/s, (b) 0.3 m/s, (c) 0.5 m/s, (d) 0.7 m/s, (e) 0.9 m/s.

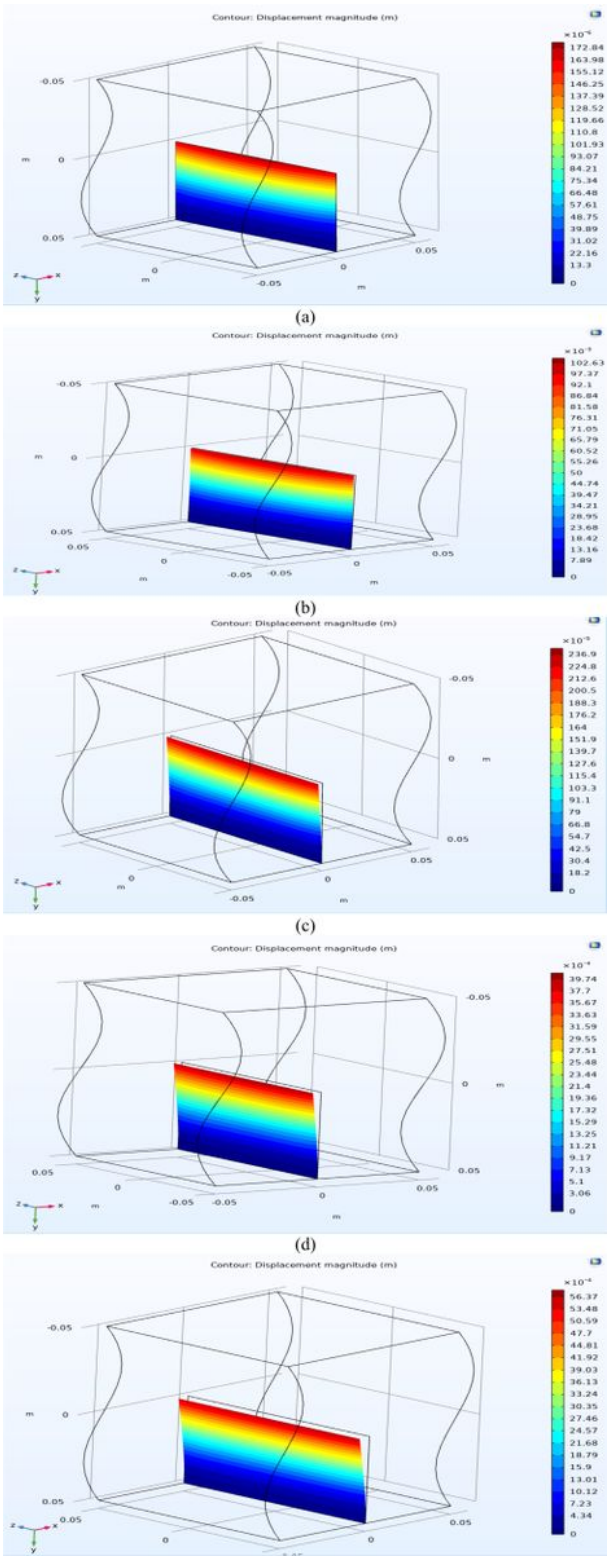

Figure 7

Deformation contour at thickness 0.5 mm. (a) 0.1 m/s, (b) 0.3 m/s, (c) 0.5 m/s, (d) 0.7 m/s, (e) 0.9 m/s.

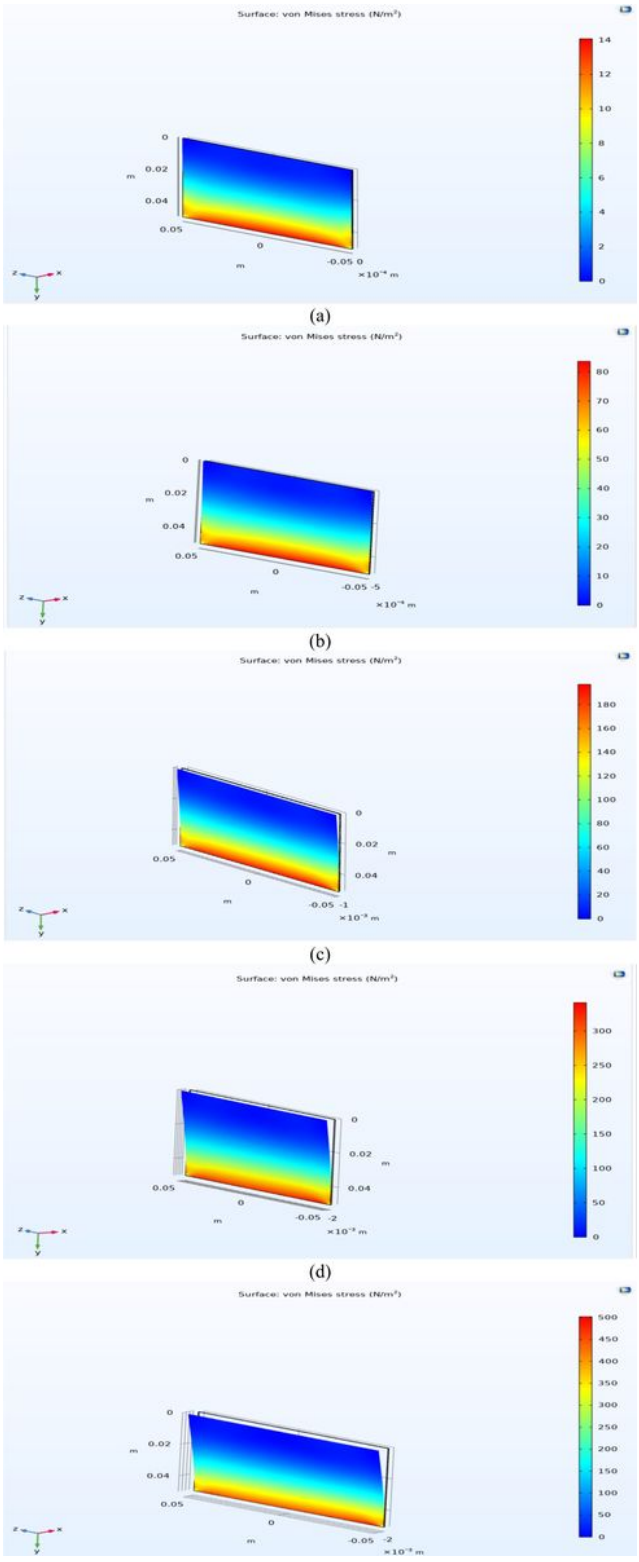

Figure 8

Von mises stress contour at thickness 0.5 mm. (a) 0.1 m/s, (b) 0.3 m/s, (c) 0.5 m/s, (d) 0.7 m/s, (e) 0.9 m/s.